Exfoliation corrosion behaviour of friction stir welded AA7136-T76 extrusions

I. Kalemba[1]*, S. Dymek[1], C. Hamilton[2], M. Wróbel[1], M. Blicharski[1]

[1] *AGH University of Science and Technology, al. Mickiewicza 30, 30-059 Kraków, Poland*
[2] *Miami University, Department of Mechanical and Manufacturing Engineering, 56 EGB, Oxford, OH 45056, USA*

Received 25 July 2008, received in revised form 21 October 2008, accepted 3 November 2008

Abstract

This research program evaluates the exfoliation corrosion properties of AA7136-T76 extrusions joined through friction stir welding (FSW). AA7136 is an aluminum alloy developed for high strength aerospace applications that also demand corrosion resistance. Extrusions were joined by FSW using a force of 26.7 kN, a welding velocity of 2.1 mm s^{-1} and a tool rotation speed of 250 RPM. Corrosion tests were performed in accordance with the requirements of ASTM G 34 and revealed a performance gradient across the weld – the weld center showing the greatest resistance to exfoliation corrosion and the thermo-mechanically affected zone adjacent to the tool shoulder showing the worst resistance to corrosion. Microscopy revealed that corrosion behavior is correlated with the distribution of $MgZn_2$ particles following supersaturation and cooling during FSW. In the weld center, coarse $MgZn_2$ particles were found on grain boundaries and within the grains alike, but near the TMAZ/HAZ boundary, large precipitates occurred on grain boundaries surrounded by precipitate free zones.

Key words: friction stir welding, aluminum, aluminum alloys, microstructure, corrosion

1. Introduction

Aluminum alloys offer a wide range of properties that make them a principal material of choice in applications where high strength-to-weight ratio is a primary requirement. This property permits design and construction of strong, lightweight structures that are particularly advantageous for automotive and aerospace applications. To meet the increasing performance demands of the industry, new grades of aluminum alloys with enhanced properties are under development. One such alloy is AA7136, manufactured by Universal Alloy Corporation. AA7136 in a conventional –T76 temper possesses superior mechanical properties compared to other commonly used 7xxx alloys, such as 7075-T6.

In addition to new alloy development, numerous efforts also concentrate on substantially reducing the manufacturing costs for components and assemblies that constitute the aircraft structure. For this reason, new manufacturing concepts, especially joining methods, are under development to replace traditional welding, brazing and riveting methods with new technologies. One such technology is friction stir welding (FSW), which introduces new concepts to the joining technology of aluminum alloys [1, 2]. Unlike traditional welding techniques, FSW is a solid-state process. Since no melting occurs during FSW, the process is performed at much lower temperatures than conventional welding techniques and circumvents many of the environmental and safety issues associated with these methods [3]. The plastic deformation and temperature profile during FSW produce a microstructure characterized by a central weld nugget surrounded by a thermo-mechanically affected zone (TMAZ) and heat affected zone (HAZ). The welded joint is fundamentally defect-free and displays excellent mechanical properties when compared to conventional fusion welds [4–6].

Aerospace structures are often subjected to adverse environmental conditions and deteriorate during their service life. Monitoring the structural health and practicing preventive maintenance is an extremely costly process. For example, deterioration due to corrosion

*Corresponding author: tel.: (4812) 617-33-94; e-mail address: kalemba@agh.edu.pl

Table 1. Chemical composition of AA7136 [8]

Element	Weight percent	
	minimum	maximum
Zn	8.4	9.4
Mg	1.8	2.5
Cu	1.9	2.5
Zr	0.10	0.20
Fe	–	0.15
Si	–	0.12
Ti	–	0.10
Mn	–	0.05
Cr	–	0.05
Other, each	0.05	
Other, total	0.15	
Al	remainder	

(in aircraft parts, Navy decks/piers) costs the United States Department of Defense $10–20 billion/year towards the detection, assessment, treatment and repair of corroded structures and components [7]. Exfoliation corrosion, or surface corrosion, of aluminum alloys is a common form of corrosion that plagues the aerospace industry. Exfoliation corrosion begins in the form of surface pits, but with time and increasing severity of the corrosive environment, the alloy will begin to delaminate, compromising the structural integrity of the system. This research paper assesses the exfoliation corrosion resistance of AA7136-T76 extrusions joined by FSW. To increase the accuracy of corrosion assessment in particular regions of the weld, a modification to the standard corrosion test, ASTM G 34, is proposed.

2. Material and experimental procedure

AA7136 contains higher levels of zinc than typical 7xxx alloys and primarily utilizes zirconium and chromium to control grain growth and recrystallization. The chemical composition of AA7136 is summarized in Table 1 [8]. The standard heat treatment for this alloy comprises supersaturation at 471 °C followed by a two-stage ageing schedule at 121 °C for 24 h and at 157 °C for 9 h to achieve the –T76 temper. Alloy extrusions with a thickness of 6.35 mm and a width of 101.6 mm were welded in the butt-weld configuration represented in Fig. 1. The welding was performed by the Edison Welding Institute in Columbus, OH, USA. As shown in the diagram, FSW occurs along the L-direction of the extrusions with a clockwise tool rotation. On the advancing side of the weld, rotation of the tool is in the same direction as the weld direction, but on the retreating side, rotation of the tool is in the opposite direction of the weld direction (the advancing and retreating sides are indicated in the figure). The diameter of the FSW tool shoulder was 17.8 mm, the pin diameter tapered linearly from 10.3 mm at the tool shoulder to 7.7 mm at the tip and the pin depth was 6.1 mm. More specific details of the tool design are proprietary to the Edison Welding Institute. The applied force was 26.7 kN, welding velocity 2.1 mm s^{-1} and the tool rotation speed 250 revolutions per minute (RPM). The microstructure of welded samples was examined by light, scanning and transmission electron microscopes (LM, TEM and SEM) on sections parallel to the panel surface (approximately 0.2 mm beneath) and also on sections perpendicular to the surface and the weld line. Before examination, the samples were electrolytically polished (solution $HClO_4 + C_2H_5OH$, temp. 12 °C, 10 V) and chemically etched in a solution of 5 ml HF, 10 ml H_2SO_4 and 85 ml water. The thin foils for TEM investigation were prepared by electropolishing in 30 % nitric acid/methanol solution at 12 V and −30 °C. The metallographic examination was supplemented by Vickers hardness measurements on a section parallel to the surface on a Zwick hardness tester with a load of 9.81 N.

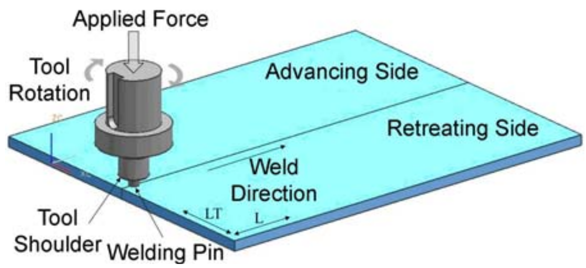

Fig. 1. Schematic of butt-weld geometry and FSW orientation.

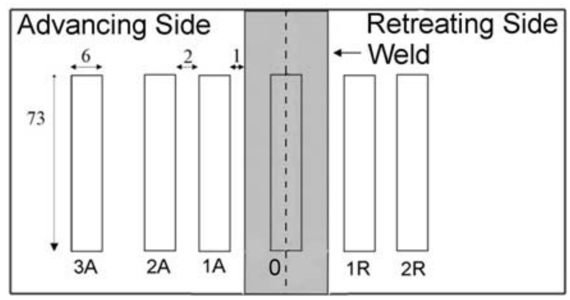

Fig. 2. Excise location of corrosion coupons from FSW panels and their designations.

For exfoliation corrosion (EXCO) examination, 73 mm long × 6 mm wide specimens were excised from the welded panel in accordance with the scheme in Fig. 2. Each sample corresponded to a unique weld area: weld center (0), TMAZ (1), HAZ near the TMAZ boundary (2) and HAZ away from the TMAZ boundary (3). The nomenclature "A" and "R" following the number assigned to a weld region corresponds to the advancing and retreating sides, respectively. The coupons were connected with each other by an electrical conductor (copper wire) to simulate the actual situation in which all weld zones are in contact with one another. This experimental configuration enabled the exfoliation corrosion resistance of the different alloy conditions produced during FSW to be evaluated and compared. Only the top surface, i.e. the surface in contact with the tool, of the coupons was exposed to corrosive attack; therefore, the remaining surfaces, i.e. the sides and back wall, were masked by a protective coating with good surface adherence. Prior to exposure, the weight of each coupon was measured, and following exposure and after drying, exfoliate product was removed from the coupon surface by the light application of a wire brush. The corroded coupons were then re-weighed in order to determine the mass loss due to exfoliation corrosion. Mass loss data, therefore, exemplified the average mass loss for specific microstructural regions associated with friction stir welding. The calculated value of mass loss per unit area represents a quantitative assessment of exfoliation corrosion resistance, in addition to the traditional ASTM classification, i.e. EA, EB, etc. The exfoliation corrosive environment prescribed in ASTM G 34 was prepared (234 g of NaCl, 50 g of KNO_3 and 6.3 ml of HNO_3 per liter of distilled water), and the coupons were subjected to a continuous immersion in the prescribed solution for 48 hours.

Because of the electrochemical nature of most corrosion processes, the relationship between solution potentials for different weld zones is of considerable importance. For this reason, in addition to EXCO tests, the coupons from the weld center, TMAZ and HAZ were subjected to corrosion potential measurements. The potentials versus Ag/AgCl electrode were measured in an aqueous solution of 34 g dm^{-3} NaCl (pH = 7.1) at room temperature (25 ℃). The samples from the same areas were also used for X-ray diffractometry and TEM investigation in order to assess the difference between phase constituents and their morphologies in various weld regions.

3. Results and discussion

Figure 3 shows a light macrograph of a typical weld cross-section and reveals a macrostructure that is uniform and essentially defect-free. There is no characteristic weld "nugget" that has been observed in many FSW investigations of other aluminum alloys [5, 6, 9, 10]. Another interesting feature of the macrostructure is the significant difference between the weld center/TMAZ boundaries on the advancing and retreating sides. On the advancing side, the weld boundary is sharp and well defined, but on the retreating side,

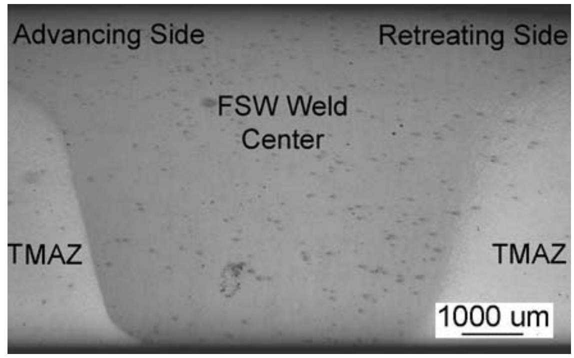

Fig. 3. Microstructure of the weld cross-section, light microscope.

the boundary gradually transitions from the macrostructure of the weld center/TMAZ to that of the HAZ/base material.

Figure 4 highlights the different microstructures from the unique weld regions: a) weld center, b) TMAZ near the HAZ boundary, c) HAZ near the TMAZ boundary and d) HAZ away from the TMAZ boundary. The notable differences pertain to precipitates as well as to grain size and shape. All changes arise due to the simultaneous action of plastic deformation and temperature profile across the weld. The microstructure of the weld center is primarily characterized by the uniform distribution of coarse precipitates, identified by X-ray phase analysis as $MgZn_2$, as shown in Fig. 5. The microstructure indicates that temperatures at the weld center were sufficient to cause coarsening and dissolution of the strengthening phases with their re-precipitation upon cooling. This observation is consistent with that of Su et al. [11], who in their study of 7050-T651 concluded that dissolution occurs within the weld center and that reprecipitation favors large precipitates, i.e. $MgZn_2$. Moving from the weld center towards the HAZ, the number of coarse precipitates decreases, and they mainly appear on grain boundaries. The decrease in the number of coarse particles suggests that limited dissolution and reprecipitation occurred in this heat-affected region. This again is consistent with the observations of Su et al. in their study of 7050-T651. In this instance, Su et al. concluded that dissolution also occured within the HAZ, but reprecipitation of small precipitates at the grain boundaries is preferred.

The grains within the weld center are very small (< 10 μm) (Fig. 6) and equiaxed, resulting from the dynamic recrystallization that occurs in this region during FSW. Within the HAZ, the grains are larger (on the order of 10–20 μm), but also equiaxed. Transmission electron microscopy revealed another pronounced difference between the microstructure of the unique weld regions. Figure 7a is a TEM micrograph of the baseline material and demonstrates

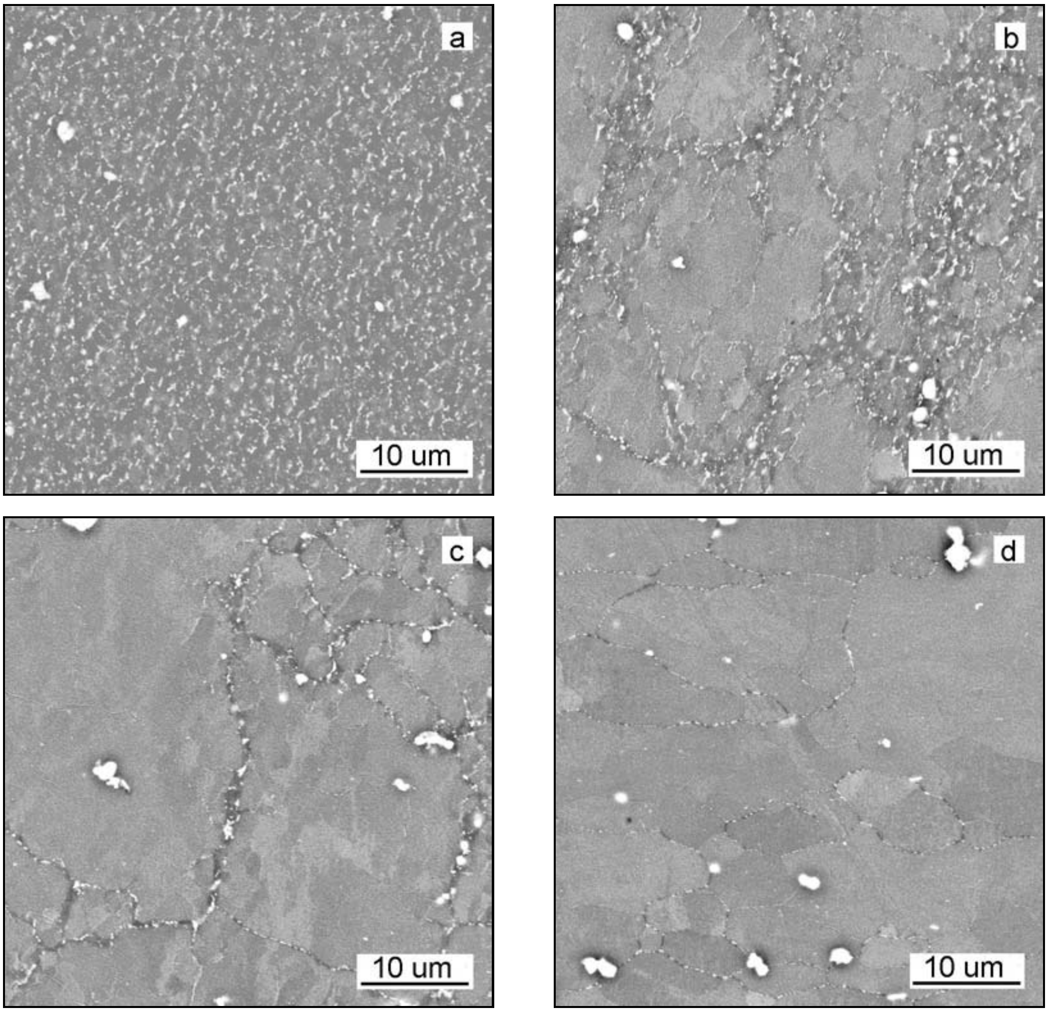

Fig. 4. Microstructures of the weld cross-section from particular weld regions: a) weld center, b) TMAZ in the HAZ boundary, c) HAZ near the TMAZ boundary, d) HAZ away from the TMAZ boundary, SEM BSE.

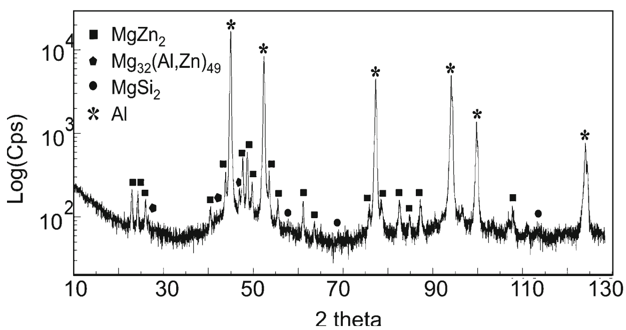

Fig. 5. X-ray diffractogram from the weld center.

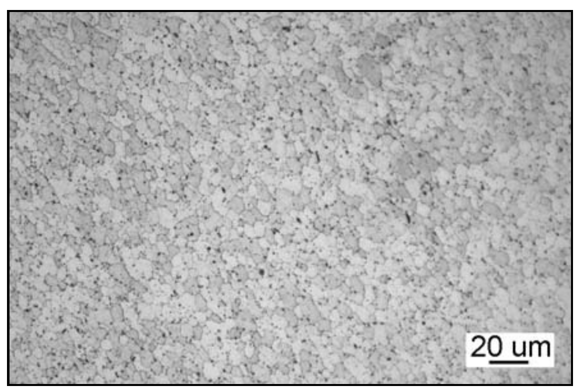

Fig. 6. Microstructure of the weld center, LM.

the high density of fine precipitates that naturally corresponds to an aluminum alloy with the strength and hardness of AA7136-T76. Within the weld center (Fig. 7b), the dispersed hardening phase appears, but its density is low, however, in the microstructure coarse $MgZn_2$ particles prevail. The microstructure of the HAZ (Fig. 7c) lacks the distribution of the coarse particles observed in the weld center, but is characterized by a high density of coarsened secondary phases. This distribution of precipitates suggests that temperatures during FSW were insufficient for dissolution and reprecipitation within this area, but were ad-

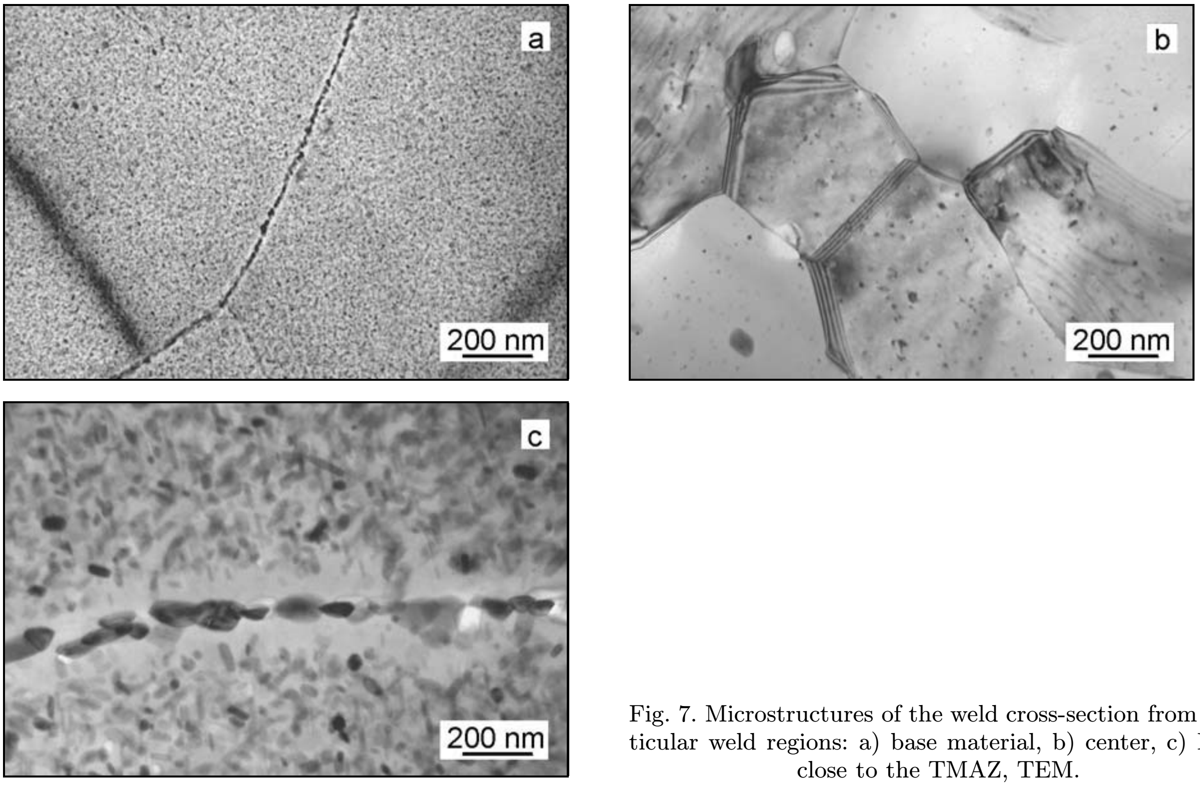

Fig. 7. Microstructures of the weld cross-section from particular weld regions: a) base material, b) center, c) HAZ close to the TMAZ, TEM.

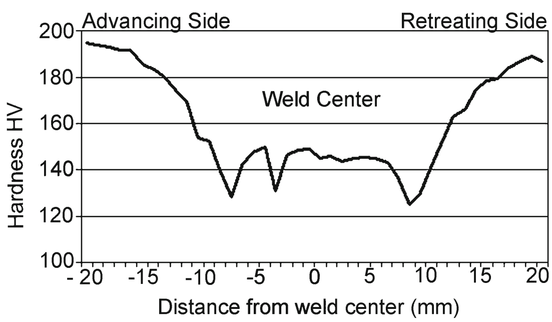

Fig. 8. Hardness profile across the weld; section parallel to the surface.

Fig. 9. Exfoliation corrosion test results.

equate to ripen the hardening phases already present within the grains. Well-defined precipitate free zones (PFZ) around the grain boundaries are also observed. Paglia and Buchheit [12] in their review of corrosion studies of friction stir welded aluminum alloys note that thermal excursions during welding promote the formation of PFZs in 7050 and that susceptibility to intergranular corrosion is correlated to coarse precipitates and wide PFZs. Temperatures within the HAZ, therefore, most likely exceed the aging temperatures of AA7136-T76, i.e. 121 ℃ and 157 ℃, but remain well below the solution heat treat temperature. The hardening phase coarsened in the HAZ as a result of the temperature increase.

The hardness profile across the weld (on the section parallel to the surface just below it) is shown in Fig. 8. The weld exhibits lower hardness than the base material, and the lowest hardness occurs in areas approximately 10 mm away from the weld centerline, i.e. the radius of the tool shoulder and the TMAZ/HAZ interface. This result correlates well with microstructural observations – the precipitates within the weld and HAZ are quite different; high density of rather small within the HAZ and a few small and other coarse within the center weld. Figure 9 presents the results of an exfoliation corrosion test performed on a specimen containing the weld and all associated microstructural regions. The weld itself actually shows very little exfoliation corrosion, receiving a rating of EA according to ASTM G 34. Within the weld, however, there are more pitted areas on the retreating side than on the advancing side, reflecting the difference in material flow between the two regions. Adjacent to the weld on both the retreating and advan-

Table 2. Summary of corrosion results

Sample	Mass loss ($g\ cm^{-2}$)	EXCO rating	E_{corr} (V)
Base	–	EB	–
3A	0.0007	EA	−0.725
2A	0.0095	EB	–
1A	0.0131	EC	−0.911
0	0.0006	EA	−0.885
1R	0.0104	EC	−0.901
2R	0.0017	EB	–

cing sides are areas of significant exfoliation corrosion (rating of EC/ED). The width of the region on the retreating side is greater than that on the advancing side, approximately 11.5 mm on the retreating side and 8.5 mm on the advancing side. Also within each corroded area, two bands are observed as the level of corrosion decreases from the TMAZ/HAZ interface toward a more corrosion-resistant area deeper into the HAZ. Outside of these corroded areas, regions of little to no exfoliation corrosion appear (rating of EA) before giving way to the baseline material, which carries an exfoliation rating of EB. These visual results are confirmed by weight loss analysis of the specimens excised according to Fig. 2. Table 2 summarizes the mass loss per unit area for the corrosion coupons of each zone investigated together with the exfoliation corrosion rating as prescribed by the ASTM standard. In addition, corrosion potential values for selected samples are presented. The mass loss data are consistent with the ASTM exfoliation corrosion ratings. The lower corrosion potentials in the TMAZ support these observations as well.

As seen in Fig. 2 and Table 2, friction stir welding results in a performance gradient across the weld with the majority of corrosion occurring within the TMAZ, but in the region adjacent to the HAZ boundary, i.e. adjacent to the tool shoulder. The increase in the resistance to exfoliation corrosion in the weld is due to the small recrystallized grains and the presence of coarse $MgZn_2$ particles that dominate the microstructure. What is more, the hardening dispersoid is no longer present in this area and thus the corrosion sensitization associated with precipitate free zones does not occur [12]. Inside the TMAZ adjacent to the HAZ the corrosion resistance is very poor. This effect may be associated with the coarsening the strengthening phase containing Zn due to the thermal excursion within the TMAZ. The loss of the hardening effect due to coarsening is confirmed by hardness measurements that show the lowest values within the TMAZ near the HAZ boundary (Fig. 8). According to [13], addition of Zn and the dissolution of the $MgZn_2$ phase shift the potential of the aluminum alloys in the anodic direction, so that a potential difference of as much as 0.24 V can exist between pure aluminum and the alloys. Furthermore, ripening within this HAZ region close to the TMAZ preferentially occurs at grain boundaries (Fig. 7c) and thus contributes to the formation of depleted zones, creating galvanic cells between the PFZs and the zinc-rich grains. The regions of enhanced exfoliation corrosion resistance result from the thermal profile effectively over aging the baseline –T76 material to a –T73 temper. As has been well established, over aged tempers such as –T73 demonstrate excellent resistance to exfoliation corrosion [14].

4. Conclusions

Friction stir welding of AA7136-T76 extrusions resulted in a performance gradient in the exfoliation corrosion resistance across the weld and the associated microstructural regions. Within the weld, the joined action of material mixing, temperature increase and dynamic recrystallization cause dissolution of the dispersed metastable phases, and upon cooling, uniformly distributed coarse $MgZn_2$ particles are formed. As such, the weld center circumvents the corrosion sensitization that occurs when coarse precipitates form on grain boundaries that are subsequently surrounded by precipitate free zones. The corrosion was most severe in the TMAZ adjacent to the HAZ boundary. TEM micrographs of this region revealed the presence of coarse grain boundary precipitates and significant PFZs. Dissolution of secondary phases is limited within this region, but as ripening occurs preferentially on the grain boundaries, a galvanic cell is established between the PFZs and the Zn-rich grain interiors. Adjacent to these regions of poor exfoliation corrosion resistance appeared areas of excellent corrosion resistance. Still within the HAZ, but well away from the TMAZ boundary, these areas benefit from a thermal excursion that effectively overages the region from the –T76 baseline temper to a –T73 temper. The retreating and advancing sides do reveal a difference in the severity of exfoliation corrosion. For example, within the weld, more pits appear on the retreating side than on the advancing side. Also, the corrosion band within the TMAZ on the retreating side is wider than that on the advancing. Though the difference in material flow and plastic deformation between the retreating and advancing sides is a likely contributor to these observations, the exact mechanisms are not known, but remain an area of active investigation.

Acknowledgements

The authors would like to acknowledge the Polish Ministry of Science and Higher Education (Grant No. N 507 458134) for their support of this research.

References

[1] THOMAS, W. M.: Great Britain Patent Application No. 9125978.8, December 1991.

[2] DAWES, C.—THOMAS, W.: TWI Bulletin, *6*, 1995, p. 124.

[3] MISHRA, R. S.—MA, Z. Y.: Material Science and Engineering R, *50*, 2005, p. 1.

[4] SUTTON, M. A.—YANG, B. C.—REYNOLDS, A. P.—YAN, J. H.: Material Science and Engineering A, *364*, 2004, p. 66.

[5] HAMILTON, C.—DYMEK, S.—BLICHARSKI, M.: Archives of Metallurgy and Materials, *52*, 2007, p. 67.

[6] SAYER, S.—CEYHUN, U.—TEZCAN, O.: Kovove Mater., *46*, 2008, p. 157.

[7] DUNMIRE, D. J.—LEE, L. A.: Defense AT&L, *33*, 2004, p. 36.

[8] GHEORGHE, I.—MALEJAN, D.: USPTO, Document No. 7214281, Universal Alloy Corporation. Anaheim, CA 2006.

[9] SATO, Y. S.—PARK, S. H. C.—KOKAWA, H.: Metallurgical and Materials Transactions A, *32*, 2001, p. 3033.

[10] SUTTON, M. A.—YANG, B.—REYNOLDS, A. P.—TAYLOR, R.: Materials Science and Engineering A, *323*, 2002, p. 160.

[11] SU, J. Q.—NELSON, T. W.—MISHRA, R.—MAHONEY, M.: Acta Materialia, *51*, 2003, p. 713.

[12] PAGLIA, C. S.—BUCHHEIT, R. G.: Scripta Materialia, *58*, 2008, p. 383.

[13] DAVIES, J. R.: Corrosion of Aluminum and Aluminum Alloys. Metals Park, OH, ASM International 1999.

[14] HATCH, J. E.: Properties and Physical Metallurgy. Metals Park, OH, ASM International 1984.